

New crystal structures of 2D Janus-type transition metal dichalcogenides

Pavel N. Gavryushkin *^{1,2,3}, Nursultan Sagatov², Ekaterina V. Sukhanova¹, Zakhar I. Popov¹, and Inna Medrish⁴

¹*Emanuel Institute of Biochemical Physics of Russian Academy of Sciences, 4 Kosygin Street, Moscow, 119334, Russian Federation*

²*Sobolev Institute of Geology and Mineralogy, Siberian Branch of Russian Academy of Sciences, prosp. acad. Koptyuga 3, 630090 Novosibirsk, Russian Federation*

³*Novosibirsk State University, Pirogova 2, Novosibirsk 630090, Russian Federation*

⁴*Samara Center for Theoretical Material Science (SCTMS), Samara State Technical University, Molodogvardeyskaya St. 244, Samara, Russia 443100*

Abstract

Transition metal dichalcogenides (TMDs) like MoS₂ or WS₂ together with graphene and its derivatives are most perspective and widely investigated 2D structures. TMDs with upper and lower layers of different chalcogen atoms were produced experimentally and was called Janus structures. In the present work, we perform the theoretical search of the new Yanus structures on the wide range of TMDCs compounds and reveal new perspective structures. Yanus structures of XTMY compositions, where X and Y are S, Se, Te, or O and TM is Mo, V, or W were considered. Two of the found structures, called T-hor and airss-1 of SMoSe and SVSe compositions, are especially perspective for experimental synthesis and practical application. These structures show dynamic stability and have enthalpies lower than enthalpy of experimentally synthesised although metastable 1T structure. For SVSe composition, enthalpy of airss-1 structure is 0.22 ev/f.u lower than that of 1T structure and 0.08 ev/f.u higher than that of 1H structure. Presence of the vanadium atoms having magnetic moment in the crystal structure implies the possible practical application as [magnetic materials (?)]. A topological analysis has shown that the discovered structures are unique and do not have analogues among structures of inorganic compounds.

*Electronic address: gavryushkin@igm.nsc.ru, p.gavryushkin@g.nsu.ru; Corresponding author

Introduction

Transition metal dichalcogenides (TMDs) represent a wide family of materials consisting of transition metal (TM: group IV, V or VI) surrounded by chalcogen atoms (Ch: S, Se or Te). TMDs crystallize in four main structural types including CdI₂, MoS₂ and FeS₂ in pyrite-type and less frequently in marcasite-type structural types [?] [A.F. Wells. Structural Inorganic Chemistry, 1986]

The first two structural types are characterized by the layered structures with Ch-TM-Ch sandwiches bonded with each other by the weak Van-der-Waals bonds and, therefore, the crystals can be exfoliated into individual stable layers [1]. These quasi-2D sandwiches attract considerable attention due to their wide range of properties [2–6]. Particularly the TMDCs with TMCh₂ stoichiometry can act as semiconductors [7], metals [8], semimetals [9, 10] or superconductors [11, 12] which make family of TMDs suitable for a lot of applications.

At ambient conditions MX₂ (M=Mo,W, X=S,Se) structures crystallize in the archetype of molybdenite structure (MoS₂) which consists of close-packed layers of chalcogen atoms placed exactly one under another along c-axis and TM atoms occupied the centers of half trigonal prismatic cavities located between the layers of chalcogen atoms. In the most stable polytype of molybdenite structure M–X–M multiplet layers similarly to *hcp* structure, which is close-packed structure with periodicity of stacking through each two layers, the structure has hexagonal symmetry and according to Ramsdell notation is denoted as 2H. In the present work we consider isolated multiplet M–X–M layers, which are usually denoted as 1H. Such a multiplet layer we will call *monolayer*, according the the accepted terminology in the 2D-community.

If one layer of chalcogen atoms in M–X–M monolayer layer is shifted, the coordination polyhedron of metal atoms changes from trigonal prism to the octahedron and the structure of CdI₂ structural type is formed. The monolayer of such a structure has trigonal symmetry and will be designated as 1T [13]. The deformed 1T structure denoted as 1T' [13] will be also considered in the manuscript. Depending on the exact chemical composition of the TMD monolayer, 1H or 1T phase is thermodynamically stable [14]. For the disulphides (as well as diselenides and ditellurides) of Mo or W, the 1T-phase is less energetically favorable than 1H-phase with the same chemical composition. However 1T structure can be obtained metastably by means of intercalation [15, 16], deformation [17] or surface functionalization [18, 19]. In contrast to Mo, W and most of the other TMs, dichalcogenides of vanadium are not known [20, 21]. However, VSe₂ structure is known in the form of 2H structure with additional V atoms located in the centers of empty trigonal prisms between the sandwiches and have the composition of Se₂V1.005 [22].

Recently a new subclass of TMDs, the so-called Janus structures, where top and bottom layers are formed by different chalcogen atoms, were produced and attracts significant interest [23, 24]. The opportunity to change the top layer of atoms opens an additional degree of freedom to manipulate the properties of TMDs. Janus TMDs have structural symmetry breaking [25, 26] resulting in Rashba spin splitting [27] and transverse dipole moment leading to large

piezoelectricity [28, 29]. The Janus structures of TMDs have a lot of potential applications, among which water-splitting [30, 31] or hydrogen evolution reaction [32, 33]. Theoretical investigations show that, as in the case of pristine monolayers, Janus TMDs with different chemical compositions can be thermodynamically stable in the 1H and 1T structures described above. Meanwhile, the different composition of the upper and bottom layers assume the possibility for the stabilization of the new structures, substantially different from 1H or 1T. This assumption was the motivation for us to perform the search for the new Janus TMDs structure with modern methods of crystal structure prediction.

Similarity and differences of the known MX₂ structures

Although H and T structures are characterized by the different coordination polyhedrons, they are similar in the manner of their interconnection. The H structure consists of trigonal prisms [MX₆] ([MX₃Y₃] for Janus structures), and T structure – of the [MX₆] octahedra (Figure 1). Each trigonal prism share all three vertical edges with the neighbouring prisms and does not share any faces. As the result, each vertex and each vertical edge of the trigonal prism is common for three prisms (Figure 1). Similarly in T structure, each octahedron share all edges inclined to the plane of sulphur atoms with neighbouring octahedra, and each vertex is common for three octahedra (Figure 1). Bond valence of Mo–S bond is nearly equal to +4/6 and there are necessary three such bonds to compensate negative charge of S₂₂[–]. Interconnection through the faces gives shorter bonds high-charged M⁴⁺ ions, increasing the energy of Coulomb interaction, and making the structure less favourable [?]. As we will show below the interconnection through the faces is also realised for predicted structures, although in most of the found structures coordination polyhedra share only common edges.

The recently found fes and fxt structures are also characterised by the trigonal prismatic coordination. However, in these structure prisms are connected not only through edges but also through the faces. The structure can be built by means of connecting through the vertices double (edge-connected) trigonal prisms (Figure ??b). In accordance with above consideration, the enthalpies of fxt and fes structures are higher than that of 1H structure, although lower than that of 1T structures. As well as in 1H and 1T structures, in fxt and fes structures, each chalcogen atoms is connected to three atoms of transition metall, providing the local charge balance (Figure ??b). As we will show below this is also not the obligatory requirement and some of the predicted structures are not charactersied by the local charge balance

1H and 1T structures provide the most uniform distribution of the chalcogen and transition metall atoms. Both nets of transition metall atoms and chalcogen atoms consist of the geometrically equal triangular loops. Edge-sharing interconnection of trigonal prisms realised in fxt and fes structures inevitably results in the appearance of the cavities bigger than that in 1H and 1T structures. In fes structure the cavities have the form of the slightly compressed cube (Figure ??). The volume of these cavities is almost two times

larger than the volume of the cavities in 1H structure (38.8 against 17.7 \AA^3). In case of fxt structure, the volume of hexagonal cavities (Figure ?? is almost 8 times larger than that in 1H structure (137.8 against 17.7 \AA^3). In contrast to trigonal prisms, the face-sharing of the right octahedra seems to be problematic for quasi 2D structure, as it results in the deviation from the flat arrangement (Figure??b – supplementary). However, as it will be shown below, the dynamically stable quasi 2D structure structures with face sharing octahedra coordination polyhedrons can be also produced.

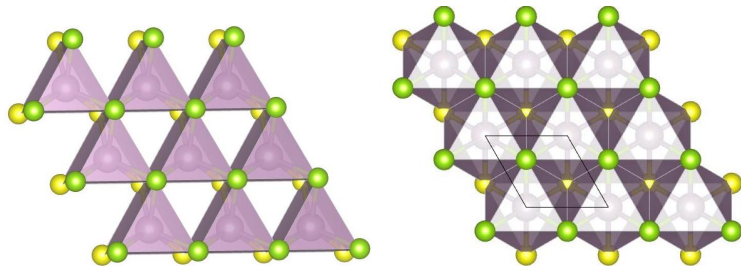


Figure 1: Packing of trigonal prisms and octahedra in H and T structures

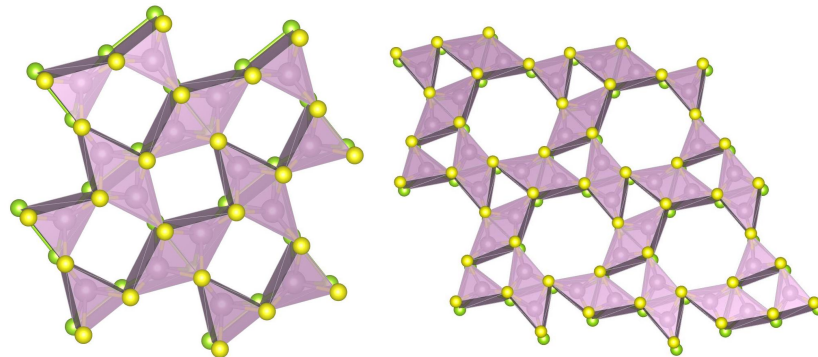


Figure 2: Packing of trigonal prisms in fes and fxt structures.

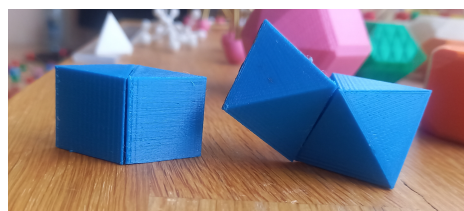


Figure 3: Two face-shared trigonal prisms and octahedra, the deviation from the horizontal plane in the last case is clearly visible

Methods

Crystal structure prediction

The search for the lowest-enthalpy monolayer structures of XMY composition was performed using evolutionary algorithms implemented in the USPEX program package [35–37] and the random sampling method implemented in the AIRSS software [38, 39].

The crystal structure search within USPEX program was performed in fixed composition mode with 2–6 formula units per unit cell. The number of structures in the first generation of the calculations was equal to 180. 50% of the structures with the lowest enthalpy were selected after the optimization and then used to produce the next generation. A new generation was produced as follow: 50% of all structures were generated by heredity, 10% – by atomic mutation, 10% – by lattice mutation, and 30% – randomly. In average, 40–47 generations were produced and relaxed. Using AIRSS program about 5000–6000 structures were randomly generated and optimized for compounds with 4 and 6 formula units per unit cell and structures with the lowest enthalpy were selected.

The total energies and forces were calculated by solving the Schrödinger equation based on projector augmented plane-wave implementation [40] of density functional theory (DFT) using the VASP program package [41, 42]. Exchange correlation effects were treated in the generalized gradient approximation (GGA) with Perdew-Bürke-Ernzerhof scheme [43].

In all crystal structure prediction calculations medium-quality optimization was performed using the conjugate gradient method [ссылка]. The energy cutoff of plane waves was set to 420 eV and 700 eV for the intermediate structures and then for the most promising of them. The first Brillouin zone was sampled according to Monkhorst-Pack scheme [44] with the density of k-point being equal to 0.5 \AA^{-1} and 0.2 \AA^{-1} , respectively.

To study a dynamic stability of predicted structures phonon dispersion spectra were calculated within the PHONOPY code [45]. We used VESTA program for crystal structures visualization [46].

Topological search

Original crystal-structural information was selected from the Inorganic Crystal Structure Database (ICSD, release 2020/2) [47] and Cambridge Structural Database (CSD, release 2021) [48].

The procedures of screening of structural-graphic data bases of compounds by the methods of the combined geometric-topological analysis with ToposPro (<http://topospro.com>) package have been used [49]. We use bold three-letter symbols of the Reticular Chemistry Structure Resource nomenclature (for the three-letter nomenclature of polyhedral and nets see Reticular Chemistry Structure Resource, <http://rcsr.anu.edu.au/>, and [50] or ToposPro Ndk-n symbols [51]) to designate the topological types of the underlying nets. The topology

of an underlying net is determined in an automated mode by comparison of a set of topological indices of the net with those for the reference nets from the ToposPro TTD collection [52].

For the topological analysis we have used only fully solved crystal structures , without errors in the determination of interatomic bonds or chemical composition, The nets of interatomic bonds were determined by the Domains methods with the program AutoCN [53]. Only strong interatomic bonds with solid angles of the faces of Voronoi-Dirihle polyhedron $\Omega \geq 5$ of the whole 4π solid angle were considered. Structures with the great values of unit cell parameters were excluded from the consideration. For instance, we did not consider polytypes of ZnS with cell parameters more than 50 Å.

Earlier the numerous structural relations between unhydrorous simple salts and even more simple binary inorganic compounds have been shown [54, 55]. Due to this well-known structural phenomena, we analyse topology not only for the complete representation, but also so the topology of the underlying net. In the complete representation, the net corresponds to the interatomic bonds of all strong bonds, while the underlying net is determined between metals and centers of ligands.

Due to the short interatomic bonds, the topologies were not determined for the crystal structures airss1, fxt, and test3.

1 Results

1.1 The new crystal structures

Table 4 show the values of enthalpies for the most energetically favorable structures, and Figure 5 phonon spectra of the most favorable structures, characterized by the absence of imaginary phonons, i.e. which are dynamically stable. The following structures are most perspective, being dynamically stable and energetically more favourable than 1T structure SMoSe composition: H-hor and airss-1 SWSe composition: H-hor and airss-1 SVSe composition: T-hor and airss-3

Below we consider their crystal structures and compare them with 1H and 1T structures.

| | SMoSe | SMoO | SMoTe | SeMoO | SeMoTe | OMoTe |
|---------|-----------------|-----------------|-----------------|-----------------|-----------------|-----------------|
| 1H | -20.8588 | -23.8327 | -19.7156 | -22.6856 | -18.9245 | -21.1902 |
| 1T | -20.1229 | -23.0531 | -19.2382 | -22.0789 | -18.3923 | -20.9359 |
| 1T' | -20.4272 | -23.2439 | -19.4668 | -22.2555 | -18.7519 | -21.2320 |
| fes | -20.0677 | -22.8773 | -19.0514 | -21.8348 | -18.3018 | -20.5800 |
| fxt | -20.0572 | -22.8076 | -19.0635 | -21.8268 | -18.3307 | -20.6590 |
| test-1 | -19.7876 | -22.5972 | -18.9050 | -21.6159 | -18.0570 | -20.2999 |
| test-2 | -20.2611 | -23.0115 | -19.2753 | -22.0542 | -18.4952 | -20.5925 |
| test-3 | -19.9359 | -22.8661 | -18.9196 | -21.8056 | -18.2335 | -20.2673 |
| H-hor | -20.0648 | -22.9347 | -19.1370 | -21.8579 | -18.3624 | -20.5998 |
| T-hor | -20.3004 | -23.0508 | -19.3146 | -22.0700 | -18.5980 | -20.8127 |
| airss-1 | -20.2308 | -23.0646 | -19.2450 | -22.1005 | -18.4711 | -21.1301 |
| airss-3 | -19.6106 | -22.3610 | -18.6248 | -21.4389 | -17.8509 | -20.4154 |

| | SVSe | SVO | SVTe | SeVO | SeVTe | OVTe |
|---------|-----------------|-----------------|-----------------|-----------------|-----------------|--------------------|
| 1H | -15.7908 | -17.3834 | -14.8886 | -16.0930 | -14.0756 | -17.4891 |
| 1T | -15.8817 | -19.5619 | -15.3259 | -18.4336 | -14.4321 | -18.1462 |
| 1T' | -15.9930 | -19.5620 | -15.3324 | -18.4428 | -14.4359 | -18.1519655 |
| fes | -15.3545 | -18.6181 | -14.7344 | -17.4218 | -13.9263 | -13.3241 |
| fxt | -15.2915 | -18.5931 | -14.7217 | -17.4922 | -13.9275 | -17.3988 |
| test-1 | -15.2359 | -17.5832 | -14.5720 | -16.7541 | -13.9923 | -17.3289 |
| test-2 | -15.4713 | -18.2459 | -14.7427 | -17.6533 | -14.0142 | -17.5650 |
| test-3 | -15.5461 | -17.2912 | -14.7832 | -16.5935 | -14.0139 | -17.2412 |
| H-hor | -15.7256 | -18.9812 | -14.9518 | -17.6724 | -14.1788 | -17.3812 |
| T-hor | -15.9091 | -19.1239 | -15.0038 | -17.8129 | -14.2606 | -17.4576 |
| airss-1 | -15.6641 | -19.0698 | -14.8539 | -17.0942 | -14.0360 | -17.6122 |
| airss-3 | -15.6467 | -19.2750 | -14.6613 | -18.0124 | -13.9868 | -17.6445 |

| | SWSe | SWO | SWTe | SeWO | SeWTe | OWTe |
|---------|-----------------|-----------------|-----------------|-----------------|-----------------|-----------------|
| 1H | -22.6659 | -25.9168 | -21.3748 | -24.6264 | -20.4873 | -22.9356 |
| 1T | -21.8487 | -25.0188 | -20.8361 | -23.8903 | -19.8942 | -22.5474 |
| 1T' | -22.2694 | -25.3082 | -21.1952 | -24.1890 | -20.4141 | -23.0212 |
| fes | -21.7743 | -24.7693 | -20.6365 | -23.5729 | -19.8245 | -22.1060 |
| fxt | -21.8355 | -24.7118 | -20.7252 | -23.6109 | -19.9329 | -22.2944 |
| test-1 | -21.5115 | -24.3282 | -20.5299 | -23.3721 | -19.7489 | -22.1465 |
| test-2 | -22.0442 | -24.9181 | -20.9534 | -23.8349 | -20.1609 | -22.4406 |
| test-3 | -21.6753 | -24.8447 | -20.7067 | -23.8419 | -19.9029 | -22.5896 |
| H-hor | -21.7550 | -24.8196 | -20.6622 | -23.6470 | -19.8179 | -22.9246 |
| T-hor | -22.0939 | -25.1586 | -20.8448 | -23.8693 | -20.1688 | -22.7002 |
| airss-1 | -22.0167 | -24.9816 | -20.9273 | -23.9214 | -20.0916 | -22.7537 |
| airss-3 | -21.5229 | -20.2019 | -20.3918 | -23.5524 | -19.5203 | -22.3072 |

Figure 4: Calculated enthalpies (eV / f.u.) of yanus XMY structures (X, Y = S, Se, Te, O, M=Mo, V, W). The structures with the lowest enthalpy for the given composition are highlighted in yellow. Structures with a lower enthalpy than the 1T (or 1H) structure are highlighted in bold.

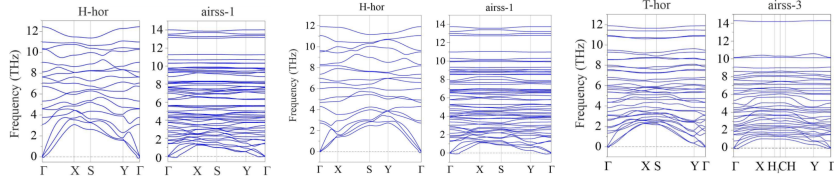


Figure 5: Calculated phonon dispersion curves for SmoSe, SWSe and SVSe.

1.1.1 Structures with trigonal prismatic coordination

To compare topologies of H, fes, and fxt structures and produce similar structures with trigonal prismatic coordination, we present the structures as different fillings of the hexagonal net of sulphur atoms (Figure 11). H-structure presents the most symmetric chess-board-like filling. The fes structure can be also considered as the chess-board filling, but with doubled triangular cell, having the form of rhombuses. After optimisation these rhombuses transform in the right squares. In fxt structure the non-filled loops are of two types. The first are three doubled triangular (rhombuses) connected through the faces, having the form of right hexagons. The second are primitive triangles. The optimisation does not sufficiently change the form of the non-filled loops, only slightly deforming hexagons.

Three new structures were produced by means of the filling of triangles in the hexagonal net of the sulphur atoms. We name them abstractly test1, test2, and test3. We failed to produce new structures obeying the local charge balance, i.e. the structures in which each vertex of the trigonal prism would be common for two other prisms. In the structure test1, each sulphur atom is common for two or four filled prisms, in test2 and test3 – for 2, 3, and 4 (Figure 11). Test3 structure is different from the other structures in that it characterised by the presence of trigonal prisms with two common faces, while in all other structures prisms has no more than one common face. Optimisation of test3 structure sufficiently affect the arrangement of sulphur atoms. In the final structure the net of sulphur atoms is not more the hexagonal one.

Presense of common edges and faces of [MoO₆] trigonal prisms in fxt, fes, test1, test2, and test3 structure results in shorter Mo–Mo distances in comparison with 1H structure, where prisms have only common edges. In H structure, Mo atoms form regular hexagonal net with all Mo–Mo bonds being equal to 3.25 Å. In fxt, fes, test1, test2, and test3 structures Mo–Mo distances varie in some range, with formation of Mo–Mo dimer connected by the stronger bonds. In optimised H structure, the Mo–Mo bonds distances are equal to 3.25 Å, in H-hor it reaches 3.08 Å, in test1 – 2.9 Å, in fxt, fes, and test2 – in average 2.62 Å, and test3 is characterised by the shortest Mo–Mo distance of 2.22 Ålength. The dimers are in turn connected in chains and layers by the weaker bonds.

Comment. fxt structure was considered as grain-boundary structure of H structure. Similarly we can describe test-1 and test-2 structure, as structures forming at grain boundary forming at contact of grains growing in opposite

direction (horizontal direction on the figure). Comment. Considering the fact that the total energies of the H phase are comparable to those of the T phase it is reasonable to expect that our proposed H structure could be found at least with the same probability as the T configuration.

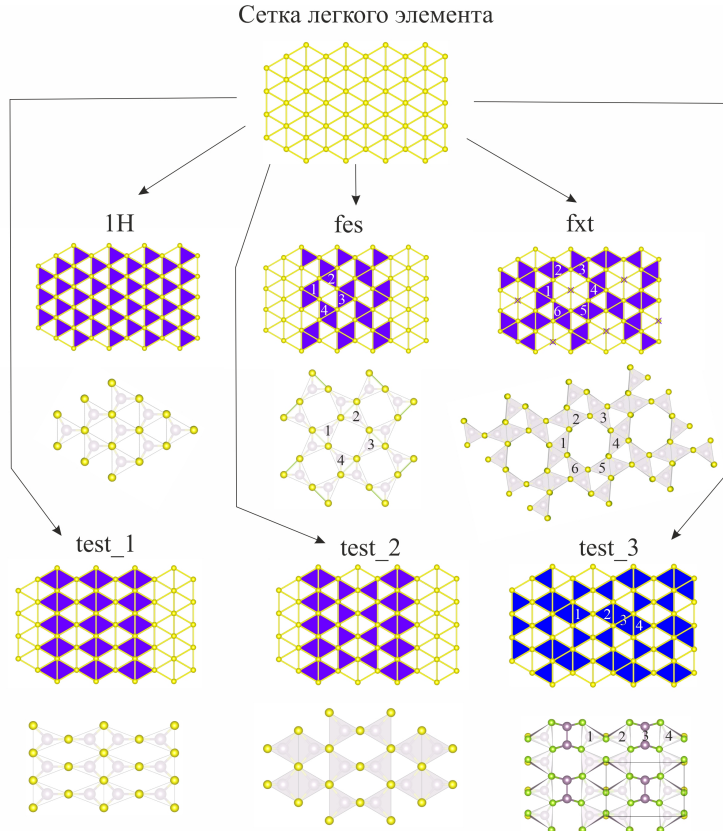


Figure 6: The initial and optimised structures of MoSSe. Тут нужно убрать связь Mo-Mo для test3 и возможно показать Mo3 в профиль

Another structure characterising by trigonal prismatic coordination was found by means of USPEX code. It is sufficiently different from all the considered above structures in that three-fold axes of trigonal prisms are parallel to the place of sulphur atoms. As the result the loops of the net sulphur atoms is not more hexagonal, but square. This structure was called H-hor (from H-horizontal)

1.1.2 Structures with octahedral coordination

As it was mentioned above T structure, composed of closely packed octahedra does not give such a flexibility as H-structure, as contact of octahedra through

the face results in the corrugation of the plane of sulphur atoms. One such a structure with face-shared octahedra have been found with AIRSS code (Figure 7). In this structure each octahedra have four common edges and one common face. The presence of the common face results in the sufficient corrugation of the layers of sulphur, in contrast to earlier considered structures. This structure was called T-hor.

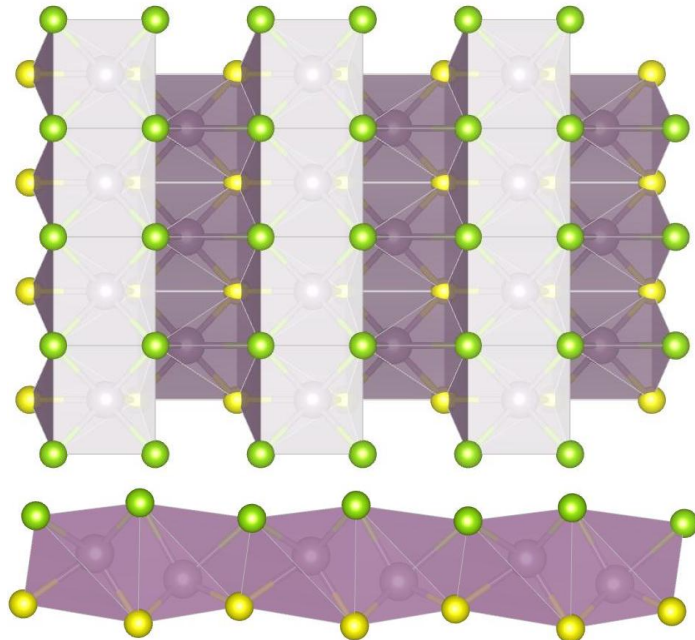


Figure 7: H-hor crystal structure perpendicular and along the layer.

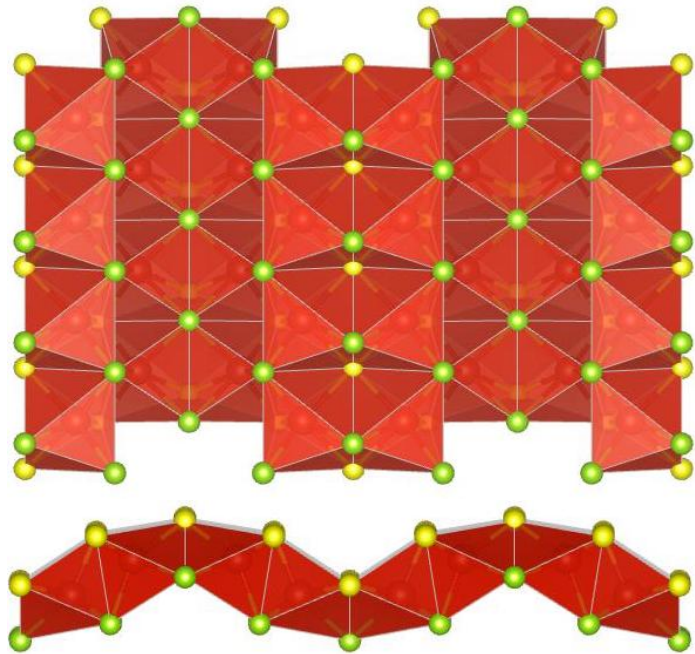


Figure 8: T-hor crystal structure perpendicular and along the layer.

1.1.3 5-coordinated crystal structure

Crystal structure with 5-coordinated Mo atoms were revealed with AIRSS code and have been called airss-1. This structure have not analogues with any structures described above. Mo atoms are surrounded by 5 chalcogenes arranged in tetragonal or ditrigonal pyramids. Two tetragonal pyramids and one ditrigonal pyramid connected through the edges are grouped in clusters. The adjacent clusters are connected through the common edges. Between clusters there are big holes, the sizes of which are comparable with the sizes of the clusters itself (Figure 9).

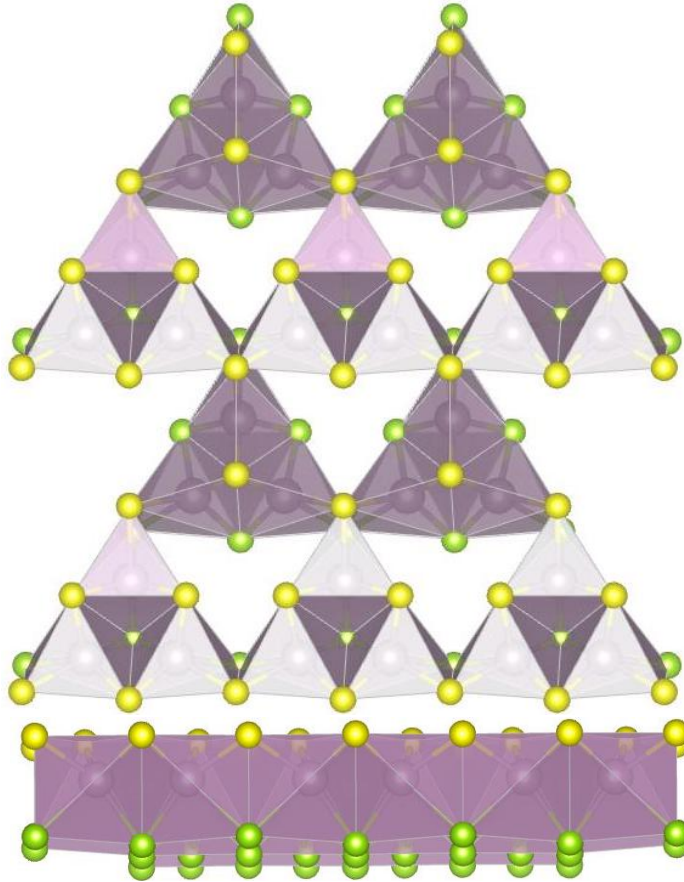


Figure 9: AIRSS-1 structure with 5-coordinated Mo atoms perpendicular and along the layer.

1.1.4 Crystal structure consisting of mixed layers of TM and Ch (chalcogene)

The structure in which TM are sufficiently shifted from the center towards upper and bottom layer was revealed for SVSe composition with AIRSS code and have been called airss-3 (Figure 10). V atoms in this structure are characterised by the coordination numbers of five and six, and coordination polyhedron have the forms of tetragonal pyramid and trigonal prism respectively. Structure can be presented as the combination of double chains, one is with the subhorizontal faces of [SV4] composition in the upper layer and another is with subhorizontal faces of [SeV4] composition in the bottom layer. Polyhedrons are connected through the common edges. Each tetragonal pyramid share six out of eight common faces and trigonal pyramid – three out of nine.

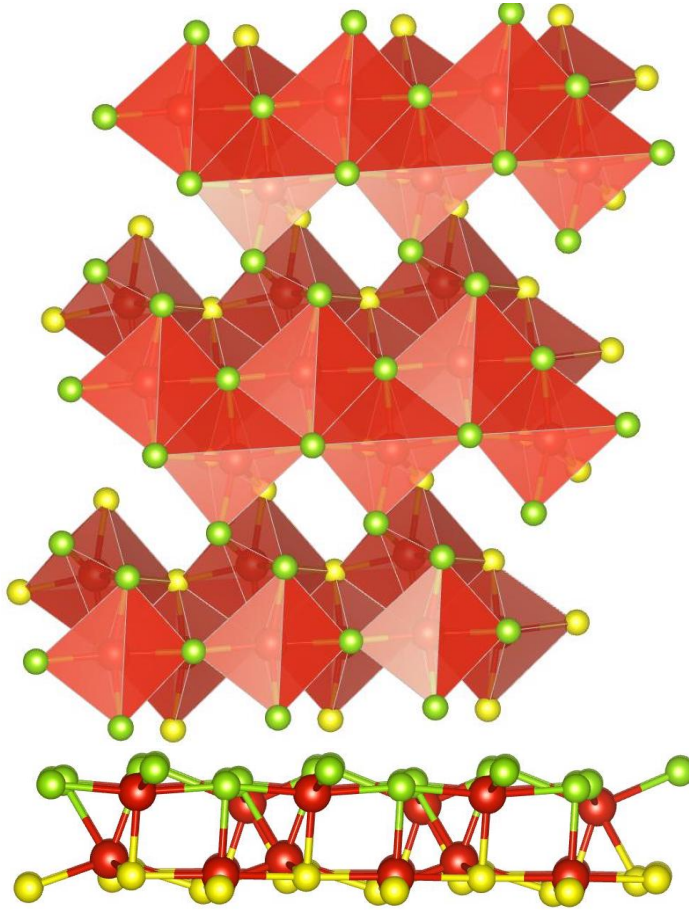


Figure 10: AIRSS-3 structure with V atoms shifted towards the planes of chalcogenes.

1.1.5 The uniqueness of the new structures

To answer the question, whether the found structures are unique or there are similar representatives in ICSD we have performed topological search. The obtained results have shown that all the found structures, except of H-hor, are unique and similar structures are not found in ICSD. The same is true about the earlier known fxt and fes structures, similar structures of which have not also been found. The H-hor structure belong to the same kgd topological type as the T structure. This means that one structure can be transformed into another without breaking the bonds. However the geometrical difference of H-hor and T structures is sufficient and transformation of one structure into the other requires changing of the coordination polyhedron from trigonal prism to octahedron.

Comment: Although TOPOS have not found such a structures, some analogues exist. Interestingly, we note that this structure resembles the structure of the recent experimentally identified monolayer C₂N-h2D[J. Mahmood, E. K. Lee, M. Jung, D. Shin, I. Jeon, S. Jung, H. Choi, J. Seo, S. Bae, S. Sohn, N. Park, J. H. Oh, H. Shin, and J. Baek, Nat. Commun. 6, 6486 (2015)]

1.1.6 Structures with trigonal prismatic coordination – possible structures of grain boundaries of 1T structures

To compare topologies of H, fes, and fxt structures and produce similar structures with trigonal prismatic coordination, we present the structures as different fillings of the hexagonal net of sulphur atoms (Figure 11). H-structure presents the most symmetric chess-board-like filling. The fes structure can be also considered as the chess-board filling, but with doubled triangular cell, having the form of rhombuses. After optimisation these rhombuses transforms in the right squares. In fxt structure the non-filled loops are of two types. The first are three doubled triangular (rhombuses) connected through the faces, having the form of right hexagons. The second are primitive triangles. The optimisation does not sufficiently change the form of the non-filled loops, only slightly deforming hexagons.

Three new structures were produced by means of the filling of triangles in the hexagonal net of the sulphur atoms. We name them abstractly test1, test2, and test3. We failed to produce new structures obeying the local charge balance, i.e. the structures in which each vertex of the trigonal prism would be common for two other prisms. In the structure test1, each sulphur atom is common for two or four filled prisms, in test2 and test3 – for 2, 3, and 4 (Figure 11). Test3 structure is different from the other structures in that it characterised by the presence of trigonal prisms with two common faces, while in all other structures prisms has no more than one common face. Optimisation of test3 structure sufficiently affect the arrangement of sulphur atoms. In the final structure the net of sulphur atoms is not more the hexagonal one.

Presence of common edges and faces of [MoO₆] trigonal prisms in fxt, fes, test1, test2, and test3 structure results in shorter Mo–Mo distances in comparison with 1H structure, where prisms have only common edges. In H structure, Mo atoms form regular hexagonal net with all Mo–Mo bonds being equal to 3.25 Å. In fxt, fes, test1, test2, and test3 structures Mo–Mo distances varie in some range, with formation of Mo–Mo dimer connected by the stronger bonds. In optimised H structure, the Mo–Mo bonds distances are equal to 3.25 Å, in H-hor it reaches 3.08 Å, in test1 – 2.9 Å, in fxt, fes, and test2 – in average 2.62 Å, and test3 is characterised by the shortest Mo–Mo distance of 2.22 Ålength. The dimers are in turn connected in chains and layers by the weaker bonds.

Comment fxt structure was considered as grain-boundary structure of H structure. Similarly we can describe test1 and test2 structure, as structures forming at grain boundary forming at contact of grains growing in oppoiste direction (horizontal direction on the figure). Comment. Considering the fact that the total energies of the H phase are comparable to those of the T phase

it is reasonable to expect that our proposed H structure could be found at least with the same probability as the T configuration.

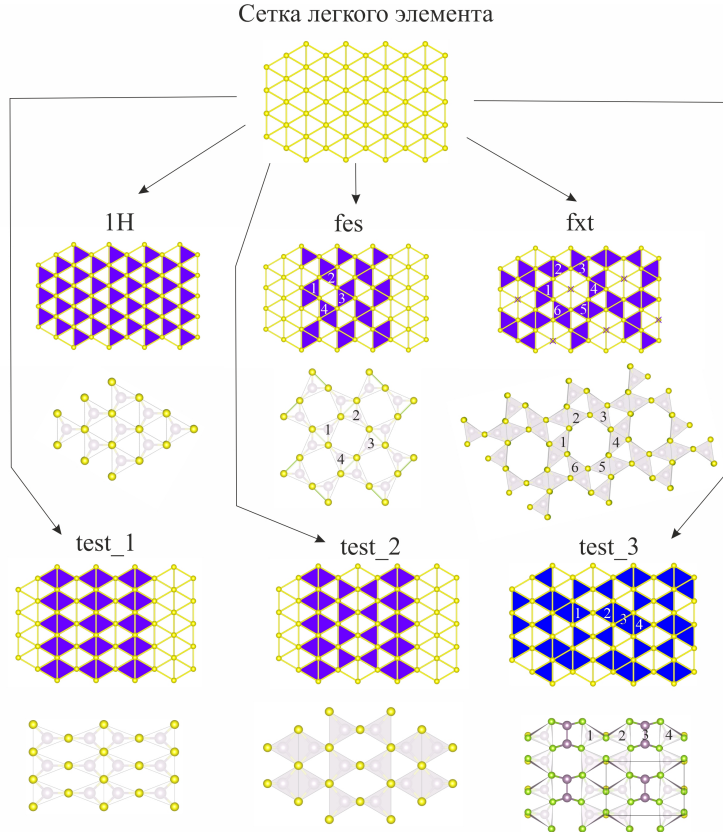


Figure 11: The initial and optimised structures of MoSSe. Тут нужно убрать связь Mo-Mo для test3 и возможно показать Mo3 в профиль

Another structure characterising by trigonal prismatic coordination was found by means of USPEX code. It is sufficiently different from all the considered above structures in that three-fold axes of trigonal prisms are parallel to the place of sulphur atoms. As the result the loops of the net sulphur atoms is not more hexagonal, but square. This structure was called H-hor (from H-horizontal)

Table 1: Calculated enthalpies of SMoSe and SVSe structures.

| Phase | Enthalpy (eV/f.u.) | | Relative H (eV/f.u.) | |
|---------|--------------------|----------|----------------------|--------|
| | SMoSe | SVSe | SMoSe | SVSe |
| 1H | -20.8588 | -15.7908 | 0.0000 | 0.2022 |
| 1T | -20.1229 | -15.8817 | 0.7358 | 0.1113 |
| 1T' | -20.4272 | -15.9930 | 0.4315 | 0.0000 |
| fes | -20.0677 | -15.3545 | 0.7910 | 0.6385 |
| fxt | -20.0572 | -15.2915 | 0.8016 | 0.7015 |
| test-1 | -19.7876 | -15.2359 | 1.0711 | 0.7571 |
| test-2 | -20.2611 | -15.4713 | 0.5977 | 0.5217 |
| test-3 | -19.9359 | -15.5461 | 0.9229 | 0.4468 |
| H-hor | -20.0648 | -15.7256 | 0.7939 | 0.2674 |
| T-hor | -20.3004 | -15.9091 | 0.5584 | 0.0838 |
| airss-1 | -20.2308 | -15.6641 | 0.6280 | 0.3289 |
| airss-3 | -19.6106 | -15.6467 | 1.2481 | 0.3463 |

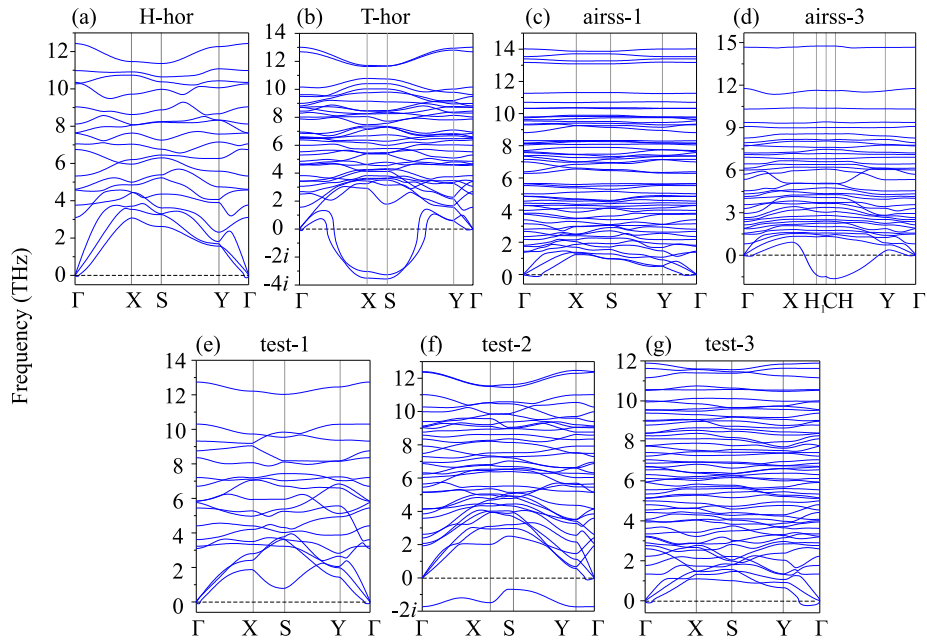


Figure 12: Phonon dispersion curves of SMoSe structures.

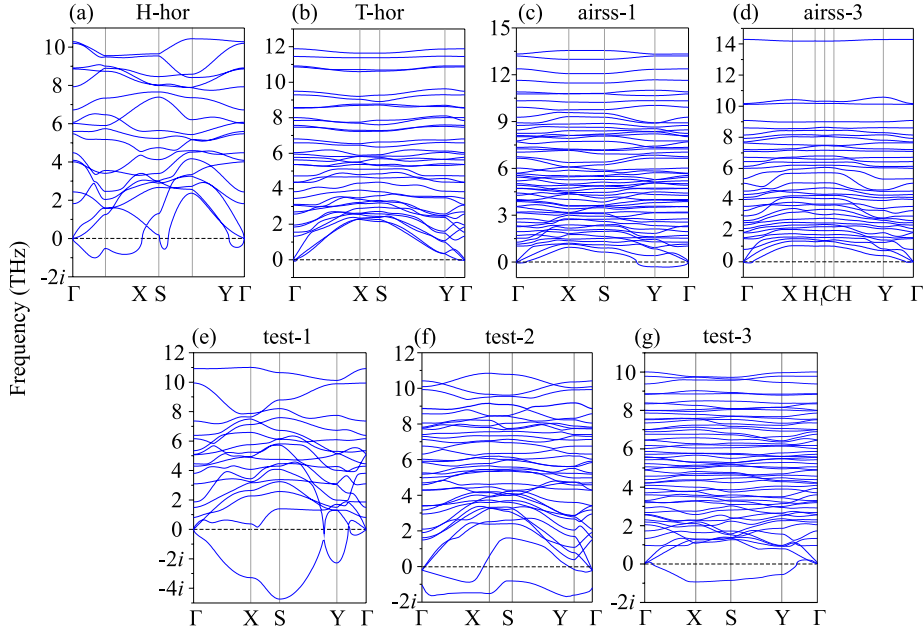


Figure 13: Phonon dispersion curves of SVSe structures.

1.2 Crystal field splitting

The crystal field theory proceeds from the fact that the nature of ligands and their location around the central ion (symmetry of the complex) reduce the degeneracy of d-orbitals and change their energy. As all investigated structures consist of transition metal atoms surrounded by ligands (chalcogen atoms), the presence of the ligands splits the d-electrons levels depending on local symmetry. Thereby the correlation between structure and electronic properties can be interpreted in terms of crystal field theory. According to crystal field theory, in an octahedral environment (1T polymorph), the d-shell splits into a low-energy triplet (t_{2g}) and a high-energy doublet (e_g). In a trigonal prismatic geometry (1H), the low-energy triplet further splits into a doublet and a singlet [<https://doi.org/10.1088/2053-1583/ab0188>]. The two polymorphs of MoS₂ have distinct electronic properties, the 1H-MoS₂ is a semiconductor and the 1T-MoS₂ is metallic. The fes-MoSSe despite the prismatic environment of TM atom becomes a semi-metal [10.1016/j.physse.2020.114485 , 10.1039/D1NA00112D] and fxt Mo and W based TMDs are gapless semiconductors or, alternatively, semimetals [10.1103/PhysRevB.93.035442]. The proposed structure airss-1 is characterized by a distorted trigonal bipyramidal local environment of the TM atom, which should make these structures more metallic due to degenerate d-orbitals. The squire pyramidal environment in airss-3 with the bare square facet of the pyramid can apply this structure for molecular sorption which makes materials in such structure perspective for sensoric and catalytic applications. In

addition, despite the fact that the surroundings of metal atoms have a prismatic environment in the geometries fxt and fes make metal atoms available for use in chemical applications due to the steric factor.

2 Conclusions

The variation of structures dictates variation electronic properties based on different d-splitting and electron filling of d-orbitals which makes it possible to manipulate electronic properties through phase transformation.

References

- [1] Zhang, Q.; Mei, L.; Cao, X.; Tang, Y.; Zeng, Z. Intercalation and exfoliation chemistries of transition metal dichalcogenides. *Journal of Materials Chemistry A* **8**, **2020**, 15417–15444.
- [2] Li, X.; Tao, L.; Chen, Z.; Fang, H.; Li, X.; Wang, X.; Xu, J.-B.; Zhu, H. Graphene and related two-dimensional materials: Structure-property relationships for electronics and optoelectronics. *Applied Physics Reviews* **4**, **2017**, 021306.
- [3] Shi, J.; Hong, M.; Zhang, Z.; Ji, Q.; Zhang, Y. Physical properties and potential applications of two-dimensional metallic transition metal dichalcogenides. *Coordination Chemistry Reviews* **376**, **2018**, 1–19.
- [4] Xi, X.; Wang, Z.; Zhao, W.; Park, J.-H.; Law, K. T.; Berger, H.; Forró, L.; Shan, J.; Mak, K. F. Ising pairing in superconducting nbse 2 atomic layers. *Nature Physics* **12**, **2016**, 139–143.
- [5] Hu, H.; Zavabeti, A.; Quan, H.; Zhu, W.; Wei, H.; Chen, D.; Ou, J. Z. Recent advances in two-dimensional transition metal dichalcogenides for biological sensing. *Biosensors and Bioelectronics* **142**, **2019**, 111573.
- [6] Pi, L.; Li, L.; Liu, K.; Zhang, Q.; Li, H.; Zhai, T. Recent progress on 2d noble-transition-metal dichalcogenides. *Advanced Functional Materials* **29**, **2019**, 1904932.
- [7] Nayeri, M.; Moradinasab, M.; Fathipour, M. The transport and optical sensing properties of mos₂, mose₂, ws₂ and wse₂ semiconducting transition metal dichalcogenides. *Semiconductor Science and Technology* **33**, **2018**, 025002.
- [8] Zhao, B.; Shen, D.; Zhang, Z.; Lu, P.; Hossain, M.; Li, J.; Li, B.; Duan, X. 2d metallic transition-metal dichalcogenides: Structures, synthesis, properties, and applications. *Advanced Functional Materials* **31**, **2021**, 2105132.

- [9] Xu, H.; Wei, J.; Zhou, H.; Feng, J.; Xu, T.; Du, H.; He, C.; Huang, Y.; Zhang, J.; Liu, Y.; et al. High spin hall conductivity in large-area type-ii dirac semimetal ptte2. *Advanced Materials* **32**, **2020**, 2000513.
- [10] Zhao, B.; Khokhriakov, D.; Zhang, Y.; Fu, H.; Karpiaik, B.; Hoque, A. M.; Xu, X.; Jiang, Y.; Yan, B.; Dash, S. P. Observation of charge to spin conversion in weyl semimetal wte 2 at room temperature. *Physical Review Research* **2**, **2020**, 013286.
- [11] Wang, L.; Fang, Y.; Huang, Y.; Cheng, E.; Ni, J.; Pan, B.; Xu, Y.; Huang, F.; Li, S. Nodeless superconducting gap in the topological superconductor candidate 2 m–ws 2. *Physical Review B* **102**, **2020**, 024523.
- [12] Hsu, Y.-T.; Vaezi, A.; Fischer, M. H.; Kim, E.-A. Topological superconductivity in monolayer transition metal dichalcogenides. *Nature communications* **8**, **2017**, 1–6.
- [13] Huang, H.; Fan, X.; Singh, D. J.; Zheng, W. Recent progress of tmd nanomaterials: phase transitions and applications. *Nanoscale* **12**, **2020**, 1247–1268.
- [14] Ataca, C.; Sahin, H.; Ciraci, S. Stable, single-layer mx2 transition-metal oxides and dichalcogenides in a honeycomb-like structure. *The Journal of Physical Chemistry C* **116**, **2012**, 8983–8999.
- [15] Kan, M.; Wang, J.; Li, X.; Zhang, S.; Li, Y.; Kawazoe, Y.; Sun, Q.; Jena, P. Structures and phase transition of a mos2 monolayer. *The Journal of Physical Chemistry C* **118**, **2014**, 1515–1522.
- [16] Wang, X.; Shen, X.; Wang, Z.; Yu, R.; Chen, L. Atomic-scale clarification of structural transition of mos2 upon sodium intercalation. *ACS nano* **8**, **2014**, 11394–11400.
- [17] Duerloo, K.-A. N.; Li, Y.; Reed, E. J. Structural phase transitions in two-dimensional mo-and w-dichalcogenide monolayers. *Nature communications* **5**, **2014**, 1–9.
- [18] Tang, Q.; Jiang, D.-e. Stabilization and band-gap tuning of the 1t-mos2 monolayer by covalent functionalization. *Chemistry of Materials* **27**, **2015**, 3743–3748.
- [19] Voiry, D.; Goswami, A.; Kappera, R.; e Silva, C. d. C. C.; Kaplan, D.; Fujita, T.; Chen, M.; Asefa, T.; Chhowalla, M. Covalent functionalization of monolayered transition metal dichalcogenides by phase engineering. *Nature chemistry* **7**, **2015**, 45–49.
- [20] Murphy, D. W.; Cros, C.; Di Salvo, F. J.; Waszczak, J. Preparation and properties of lixvs2 (0. Itoreq. x. Itoreq. 1). *Inorganic Chemistry* **16**, **1977**, 3027–3031.

- [21] Le Nagard, N.; Katty, A.; Collin, G.; Gorochov, O.; Willig, A. Elaboration, structure cristalline et propriétés physiques (transport, susceptibilité magnétique et rmn) du spinelle cuv₂s₄. *Journal of Solid State Chemistry* **27**, **1979**, 267–277.
- [22] Rigoult, J.; Guidi-Morosini, C.; Tomas, A.; Molinie, P. An accurate refinement of 1t-v se₂ at room temperature. *Acta Crystallographica B* **38**, **1982**, 1557–1559.
- [23] Lu, A.-Y.; Zhu, H.; Xiao, J.; Chuu, C.-P.; Han, Y.; Chiu, M.-H.; Cheng, C.-C.; Yang, C.-W.; Wei, K.-H.; Yang, Y.; et al. Janus monolayers of transition metal dichalcogenides. *Nature nanotechnology* **12**, **2017**, 744–749.
- [24] Zhang, J.; Jia, S.; Kholmanov, I.; Dong, L.; Er, D.; Chen, W.; Guo, H.; Jin, Z.; Shenoy, V. B.; Shi, L.; et al. Janus monolayer transition-metal dichalcogenides. *ACS nano* **11**, **2017**, 8192–8198.
- [25] Li, F.; Wei, W.; Zhao, P.; Huang, B.; Dai, Y. Electronic and optical properties of pristine and vertical and lateral heterostructures of janus mosse and wsse. *The journal of physical chemistry letters* **8**, **2017**, 5959–5965.
- [26] Van Thanh, V.; Van, N. D.; Saito, R.; Hung, N. T.; et al. First-principles study of mechanical, electronic and optical properties of janus structure in transition metal dichalcogenides. *Applied Surface Science* **526**, **2020**, 146730.
- [27] Hu, T.; Jia, F.; Zhao, G.; Wu, J.; Stroppa, A.; Ren, W. Intrinsic and anisotropic rashba spin splitting in janus transition-metal dichalcogenide monolayers. *Physical Review B* **97**, **2018**, 235404.
- [28] Dong, L.; Lou, J.; Shenoy, V. B. Large in-plane and vertical piezoelectricity in janus transition metal dichalcogenides. *ACS nano* **11**, **2017**, 8242–8248.
- [29] Li, R.; Cheng, Y.; Huang, W. Recent progress of janus 2d transition metal chalcogenides: from theory to experiments. *Small* **14**, **2018**, 1802091.
- [30] Xia, C.; Xiong, W.; Du, J.; Wang, T.; Peng, Y.; Li, J. Universality of electronic characteristics and photocatalyst applications in the two-dimensional janus transition metal dichalcogenides. *Physical Review B* **98**, **2018**, 165424.
- [31] Ma, X.; Wu, X.; Wang, H.; Wang, Y. A janus mosse monolayer: a potential wide solar-spectrum water-splitting photocatalyst with a low carrier recombination rate. *Journal of Materials Chemistry A* **6**, **2018**, 2295–2301.
- [32] Er, D.; Ye, H.; Frey, N. C.; Kumar, H.; Lou, J.; Shenoy, V. B. Prediction of enhanced catalytic activity for hydrogen evolution reaction in janus transition metal dichalcogenides. *Nano letters* **18**, **2018**, 3943–3949.

- [33] Zhou, Z.; Niu, X.; Zhang, Y.; Wang, J. Janus mosse/wsete heterostructures: a direct z-scheme photocatalyst for hydrogen evolution. *Journal of Materials Chemistry A* **7**, **2019**, 21835–21842.
- [34] Pauling, L. The principles determining the structure of complex ionic crystals. *Journal of the american chemical society* **51**, **1929**, 1010–1026.
- [35] Oganov, A. R.; Glass, C. W. Crystal structure prediction using ab initio evolutionary techniques: Principles and applications. *The Journal of Chemical Physics* **124**, **2006**, 244704.
- [36] Oganov, A. R.; Lyakhov, A. O.; Valle, M. How evolutionary crystal structure prediction works—and why. *Accounts of Chemical Research* **44**, **2011**, 227–237.
- [37] Lyakhov, A. O.; Oganov, A. R.; Stokes, H. T.; Zhu, Q. New developments in evolutionary structure prediction algorithm uspex. *Computer Physics Communications* **184**, **2013**, 1172–1182.
- [38] Pickard, C. J.; Needs, R. J. High-pressure phases of silane. *Physical Review Letters* **97**, **2006**, 045504.
- [39] Pickard, C. J.; Needs, R. J. Ab initio random structure searching. *Journal of Physics: Condensed Matter* **23**, **2011**, 053201.
- [40] Blöchl, P. E. Projector augmented-wave method. *Physical review B* **50**, **1994**, 17953.
- [41] Kresse, G.; Furthmüller, J. Efficient iterative schemes for ab initio total-energy calculations using a plane-wave basis set. *Physical Review B* **54**, **1996**, 11169–11186.
- [42] Kresse, G.; Furthmüller, J. Efficiency of ab-initio total energy calculations for metals and semiconductors using a plane-wave basis set. *Computational Materials Science* **6**, **1996**, 15–50.
- [43] Perdew, J. P.; Burke, K.; Ernzerhof, M. Generalized gradient approximation made simple. *Physical Review Letters* **77**, **1996**, 3865.
- [44] Monkhorst, H. J.; Pack, J. D. Special points for brillouin-zone integrations. *Physical review B* **13**, **1976**, 5188.
- [45] Togo, A.; Tanaka, I. First principles phonon calculations in materials science. *Scripta Materialia* **108**, **2015**, 1–5.
- [46] Momma, K.; Izumi, F. Vesta 3 for three-dimensional visualization of crystal, volumetric and morphology data. *Journal of applied crystallography* **44**, **2011**, 1272–1276.

- [47] Belsky, A.; Hellenbrandt, M.; Karen, V. L.; Luksch, P. New developments in the inorganic crystal structure database (icsd): accessibility in support of materials research and design. *Acta Crystallographica Section B: Structural Science* **58**, **2002**, 364–369.
- [48] Groom, C. R.; Bruno, I. J.; Lightfoot, M. P.; Ward, S. C. The cambridge structural database. *Acta Crystallographica Section B: Structural Science, Crystal Engineering and Materials* **72**, **2016**, 171–179.
- [49] Blatov, V. A.; Shevchenko, A. P.; Proserpio, D. M. Applied topological analysis of crystal structures with the program package topospro. *Crystal Growth & Design* **14**, **2014**, 3576–3586.
- [50] O'Keeffe, M.; Peskov, M. A.; Ramsden, S. J.; Yaghi, O. M. The reticular chemistry structure resource (rcsr) database of, and symbols for, crystal nets. *Accounts of chemical research* **41**, **2008**, 1782–1789.
- [51] Alexandrov, E.; Blatov, V.; Kochetkov, A.; Proserpio, D. Underlying nets in three-periodic coordination polymers: topology, taxonomy and prediction from a computer-aided analysis of the cambridge structural database. *CrystEngComm* **13**, **2011**, 3947–3958.
- [52] Alexandrov, E. V.; Shevchenko, A. P.; Blatov, V. A. Topological databases: why do we need them for design of coordination polymers? *Crystal Growth & Design* **19**, **2019**, 2604–2614.
- [53] Blatov, V. A method for topological analysis of rod packings. *Structural Chemistry* **27**, **2016**, 1605–1611.
- [54] Blatov, V. A. Crystal structures of inorganic oxoacid salts perceived as cation arrays: a periodic-graph approach. *Inorganic 3D Structures* **2011**, 31–66.
- [55] Medrish, I. V.; Eremin, R. A.; Blatov, V. A. From simple to complex: Design of inorganic crystal structures with a topologically extended zintl-klemm concept. *The Journal of Physical Chemistry Letters* **11**, **2020**, 8114–8120.